Received: 14 July 2023 | Revised: 18 September 2023 | Accepted: 12 October 2023 | Published online: 13 October 2023

RESEARCH ARTICLE

Journal of Data Science and Intelligent Systems
2023, Vol. 00(00) 1–6
DOI: 10.47852/bonviewJDSIS32021359

BON VIEW PUBLISHING

Design of a Multilayer Perceptron Network Based on the Normalized Histogram to Develop Yields Predictive Model

Zena H. Khalil[1],* and Alaa Hussein Khaleel[2]

[1]*College of Computer Science and Information Technology, University of Al-Qadisiyah, Iraq*

[2]*College of Energy and Environmental Science, Al-Karkh University for Science, Iraq*

Abstract: This article presents a multilayer perceptron (MLP) network for spatio-temporal remote sensing analysis of satellite image time series for a yield prediction model. This article illustrates the model for crop yield prediction from the spatial cumulation of normalized difference vegetation index (NDVI) image time series at the province level. The methodological framework comprises the transformation of each NDVI image into a histogram to ensure no loss of information in the mapping of high-dimensional/unstructured NDVI images into pixels consideration, to be then used in training the MLP. The research work also includes an analysis of several activation functions for the hidden layer and testing their consequences on accuracy, including Radial-Basis (RadBas), Logarithmic-Sigmoid (LogSig), and Hyperbolic-Tangent Sigmoid (TanSig), which depend mainly on exponential functions and limit the amplitude of the output. The proposed approach was utilized to predict the winter crop yield in Diwaniyah-Iraq province, one of the main agriculture regions, whose economy considerably depends on crop production. It can also be extended to other crops and other regions in Iraq. The proposed methodology showed the ability to predict the crop yield around 7–9 weeks before harvest. It also outperformed the performance of traditional approaches by transforming the input into a more convenient form that reflects more useful information. The results show that the proposed model provides efficient accuracy (determination coefficient $R^2 > 0.85$ and error level < 0.24).

Keywords: artificial neural network, crop prediction, normalized difference vegetation index, Diwaniyah-Iraq

1. Introduction

The country of Iraq is known as one of the oldest agricultural countries known in the world. Nowadays, agriculture is an important source of employment and livelihood, despite the fact this sector is no longer the most important contributor to the country's economy. However, one-third of the overall population lives in rural areas in which agriculture is the main significant source of livelihoods [1].

Approximately 26% of the country's total region is cultivable and 70%–85% of cultivated crops are dedicated to planting wheat and barley in any given year [2], which is produced either under rainfed conditions or irrigated by the Tigris and Euphrates rivers, and 67% of wheat/barley comes from irrigation production. Figure 1 shows the wheat/barley production in Diwaniyah (2001–2019).

The challenge in yield prediction is to get accurate prediction at a higher spatial resolution, such as at a province or even household level. Therefore, the researchers in such situations tend to use very high-resolution imagery such as Sentinel-2 with 10–20 m resolution [2]. But the high-resolution imagery has a huge amount of data and this means massive amounts of computation and time-consuming, in addition to high cost. On another side, high-resolution satellite imagery provides an inadequate temporal duration of observations causing in reducing the accuracy of empirical models, that is

Figure 1
Wheat/barley production in the study area (2001-2020)

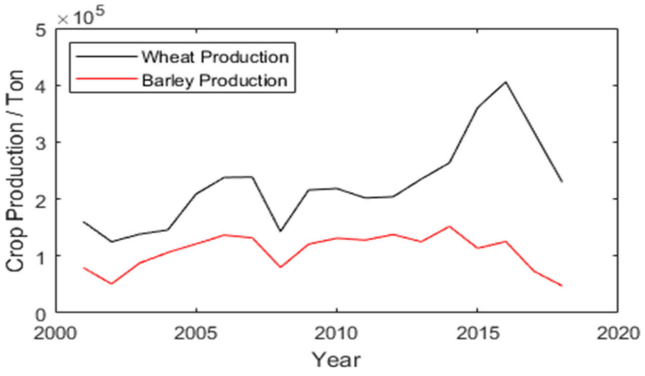

*Corresponding author. Zena H. Khalil, College of Computer Science and Information Technology, University of Al-Qadisiyah, Iraq, Email: zena.khalil@qu.edu.iq

because their launching was in the only last few years. The MODIS sensor, which is a Moderate Resolution Imaging Spectroradiometer, was our satellite source in this study. It was originally designed to provide data on vegetation and land cover maps. It also has high spectral and temporal resolution causing a great quality of normalized difference vegetation index (NDVI) product for crop growth monitoring and crop yield estimation, that is, due to narrow spectral bands of MODIS, which minimize the impact of water-vapor absorption in the near-infrared (NIR) band, resulting in the sense of the red band data to chlorophyll. This gives NDVI the ability to monitor crop growth conditions and describe the variability of yield within the growing season [3, 4]. Conventionally, the statistical methods had been used for yield prediction, but such methods showed limitations in cases when must consider many factors and relationships [5]. For handling the complicated factors and relationships in crop yield prediction, artificial neural networks (ANNs) have been applied in our work.

The work aimed to answer the following questions: (i) Is the use of NDVI satellite data will achieve predicting wheat and barley yield in the irrigated area? (ii) How does ANN method achieve a result in modeling crop yield? (iii) Examine which exponential activation function give best results for proposed architectures?

However, the main contributions of this article are introducing a predicting methodology work with the entire pixels distribution in subregions over province directly as features for learning and check the validity of the proposed approach in a study area in the Diwaniyah-Iraq province.

2. Material and Methods

2.1. Study area

The study area is the province of Diwaniyah-Iraq. It is located in the middle south of Iraq between latitudes (30.5°–32.5°)N and longitudes (44.5°–46°)E. The geological formations consist of a sedimentary plain, flat sand land, the western plateau in addition to Al-Dalmaj marsh. The majority of the province area is represented by sedimentary plains approximately 77% of which is the most populated area of Iraq and suitable for agriculture, this encouraged cultivation in that region, especially the cultivation of crops [6]. In this work, we focus on the main wheat and barley cropping regions in Diwaniyah, where the growing season of these crops is usually from November to March.

2.2. Datasets and preprocessing

For analysis and modeling of this work, we collected data from several sources, including province boundaries data, annual crop yield data for wheat and barley, cropping area, and satellite data. According to the data availability, our study period was from 2001 to 2020. In this study, MODIS-NDVI data/product MOD13Q1 [7] was adopted to predict the wheat and barley yield in study area; due to the success achieved by MODIS-NDVI not only in crop yield prediction and estimation but also in various studies concern with crop such as crop mapping [8], land use/land cover change [9] and crop classification [10].

The MOD13Q1 images were obtained from the USGS Earth Explorer user interface developed by the United States Geological Survey, every 16 days along the growing season from November to May resulting in 12 NDVI images for every year during the study period. These images are scaled by a factor of 0.0001 and then the cropland pixels are extracted from each NDVI image using cropland shapefiles for each year created using a MODIS land cover/product MCD12Q1 [11, 12]. Then the NDVI pixel values within each masked area less than 0.1 were removed, which deliberately excluded from future calculations the pixels of non-vegetation origin related to water objects and urban development. Then entire masked area for each year is divided into three NDVI regions. Figure 2(a) shows the distribution of croplands and other basic landscapes of Diwaniyah province in 2015, Figure 2(b) shows the cropland mask for year 2015, and Figure 2(c) shows the division of cropland area into subregions, which are surrounded by yellow boxes.

Figure 2
(a) Classification of the landscapes for 2015 year, (b) the shapefile of Diwaniyah province for 2015 year, and (c) distribution of subregions of Diwaniyah province

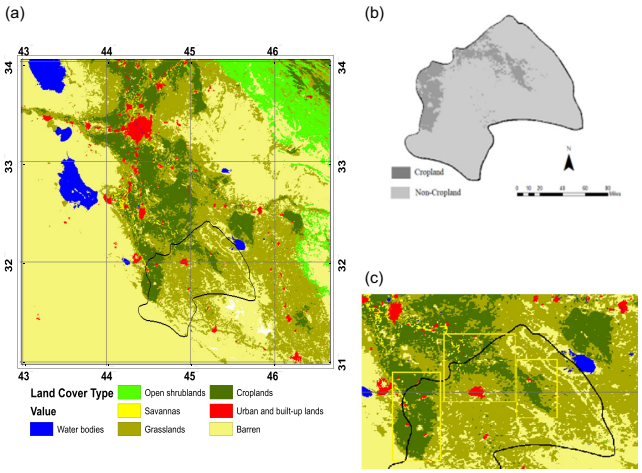

2.3. Temporal data analysis

Before applying any learning algorithms, it must be to do a statistical data analysis to select the most appropriate independent input variables in addition to dimensionality reduction [13]. In this work, a temporal analysis was conducted to determine the best time of year to make an accurate yield prediction with relatively long enough lead time.

The analysis was performed by tracking the average of NDVI in each region during growing season through all study period. As shown clearly in Figure 3 that the maximum of NDVI starts in February, reaches a peak in March, and then decreases gradually until the end of growing season. Therefore, only the satellite images in February were considered in the prediction model. Indeed, this caused a data reduction from 684 images to only 114 images (by taking only two images from February for each year of the study period) to be analyzed for the prediction process.

Figure 3
Temporal analysis

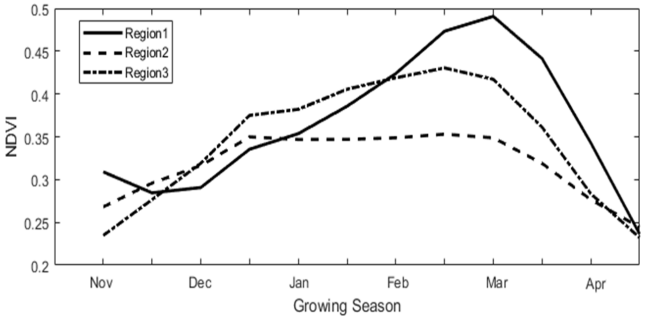

3. Proposed MLP Model Based on the Histogram Consideration

3.1. Preliminary

To take into account the dimensionality reduction of NDVI images, we preferred to use a histogram technique. Unlike the rest of the existing approaches, which preferred to use the mean value of NDVI pixels over regions or provinces and introduced it as a feature into MLP. However, these approaches have low computing complexity but are inclined to skip the detailed differences in the region [14]. On the other hand, it is difficult to feed all NDVI pixels into neural networks directly, because of hard to extract useful features from huge and unstructured data. We overcome this problem by transforming each NDVI image into a histogram to ensure no loss of information in the mapping of high-dimensional images into pixel counts histograms where the histogram is particularly useful when dealing with a large number of observations.

The problem with the histogram is that it contains no information about the spatial arrangement of pixels in the image [15]. Therefore, we divided the entire masked cropland area into three NDVI regions to take into account the spatial heterogeneity of NDVI, as shown previously in Figure 2(c). Once the three regions were delineated, pixel values for the NDVI image of each region were extracted and histograms were generated. NDVI image uses a larger range of values causing the growing number of histogram entries and making it less practical, so for each histogram curve, we generated 10 gradations (buckets or bin) that represented different ranges of NDVI distributions in the date of the corresponding NDVI image with a uniform interval (width) and reveal the underlying shape of the distribution, resulting in 20 gradations (buckets) of NDVI distributions in February. That is because of the fact of Sturge's rule, Equation (1):

$$Number\ of\ gradations(bin) = 1 + 3.322\ \log N \tag{1}$$

where N represents the number of NDVI pixels in the region.

Finally, the frequency value of each bucket was divided by the total number of pixels contained within that bucket, i.e., divide it by the interval length, in order to get a normalized histogram for the first and second half of February for each of the three regions and introduced it as features to MLP neural network.

3.2. Mathematical model

For learning a predictive model that attempts to predict crop yields for any specific district (province) over a given growing season and year, the feature space for such a model is a collection of NDVI images for a cropland area A. Each image I in A correlates to a certain subregion s and two-time steps (2 images in each year). Therefore, for each ground truth crop yield y, we introduce the feature set as in Equations (2)–(6):

$$\{(I_1^1 \ldots I_s^1, I_1^2 \ldots I_s^2)_1, \ldots, (I_1^1 \ldots I_s^1, I_1^2 \ldots I_s^2)_n\} \to y,\ y \in \mathbb{R}^+,\ n, s \in \mathbb{Z}^+ \tag{2}$$

The histogram h for each image I with NDVI gradations at each location (u, v) in the range $I(u, v) \in [0.1, K]$ can be represented as:

$$h(i) = card\{(u, v) | I(u, v) = i\} \qquad \forall i : 0.1 \le i \le K \tag{3}$$

The resulting of this computation is a 1-D vector h, to convert it into binned histogram with B bins(buckets), each bin h(b) contains the number of NDVI gradations within the interval $[ab, ab + 1]$

$$h(b) = card\{(u, v) |\ a_b\ \le I(u, v) < a_{b+1}\}$$

$$\forall b : 1 \le b \le B \tag{4}$$

The normalized histogram will be

$$H(b) =\ h(b)/\Delta(a_b, a_{b+1}) \qquad \forall b : 1 \le b \le B \tag{5}$$

So, the predictive model will be

$$\{(H_1^1 \ldots H_s^1, H_1^2 \ldots H_s^2)_1, \ldots, (H_1^1 \ldots H_s^1, H_1^2 \ldots H_s^2)_n\} \to y$$

$$,\ y \in \mathbb{R}^+\ ,n, s \in \mathbb{Z}^+ \tag{6}$$

3.3. Transformation

In general, the ANN may produce more accurate and reliable results with added two phases consisting of preprocessing and postprocessing into the fundamental process. The MLP networks, with some sort of activation function in the hidden layer, may become saturated when the net input is greater than a specific value. This means that the units are only sensitive to inputs within a somewhat limited range. This issue can be solved by employing a normalization for the input/output datasets, in order to make the network produce outcomes within a specific normalized range. Also, to deal with different variables despite their scale and ensure that the network outputs are in a sensible (appropriate) range. Therefore, a normalization algorithm (or scaling algorithm) must be applied to datasets.

In this work, the input/output datasets scaled linearly to be transformed into a range of [0,1], according to Haykin [16], Equation (7):

$$x_n = \frac{x - \min(x)}{\max(x) - \min(x)} \tag{7}$$

3.4. Multilayer layer perceptron

3.4.1. Architecture

MLP network architecture, in the aspect of function approximation, is well known in predicting problems [17] and widely applied in diverse function estimating problems in different applications [18]. Therefore, in this work, we preferred to use MLP in order to predict crop yield.

The structural design in the application of ANN is a crucial step because the number of the hidden layer is critical for the network's capability for learning the characteristics of the training dataset, while the number of nodes in the hidden layer(s) stands for the complexity and ability of the ANN to describe underlying structures among a training data. Hence, it should be large enough for the accurate representation of the problem and low enough for generalization capabilities.

Generally regarded that a single hidden layer must be sufficient for most problems because a MLP with one hidden layer can approximate any function, so most of the ANNs used in remote sensing are based upon a single hidden layer MLP [19]. Therefore, in this work, we utilize a MLP with a single hidden layer. According to Karul et al. [20], the feedforward backpropagation ANN with sufficient hidden layer neurons number can approximate any function, so it is necessary to assign only a minimum number of neurons (regularization) that is just sufficient for learning the system in order to prevent an overfitting problem. Corresponding to Mas and Flores [19] and Karul et al. [20], we used a reliable trial-and-error strategy and found that assigning five neurons in the hidden layer is most proper to our model.

The learning algorithm enables the network to adjust the weights between successive training epochs. The most popular learning strategy developed for MLP is the backpropagation learning algorithm. The Levenberg–Marquardt backpropagation is usually more efficient, highest convergence speed, and outperforms other backpropagation learning algorithms [21, 22]. It is also characterized as having the fastest convergence for medium-low-sized feedforward neural networks, so we used it as a learning function in the suggested model.

In this work, several activation functions were examined for hidden layer and tested their consequences on accuracy, including Radial-Basis (RadBas), Logarithmic-Sigmoid (LogSig), and Hyperbolic-Tangent Sigmoid (TanSig), which depend mainly on exponential function and limit the amplitude of output in [−1,1] or [0,1], (Figure 4). The linear transfer function is typically used in literature for function approximation in the output layer with regression tasks (in terms of prediction) [16], so in the suggested model, the (purelin) was used for the output layer.

Figure 4
Activation functions

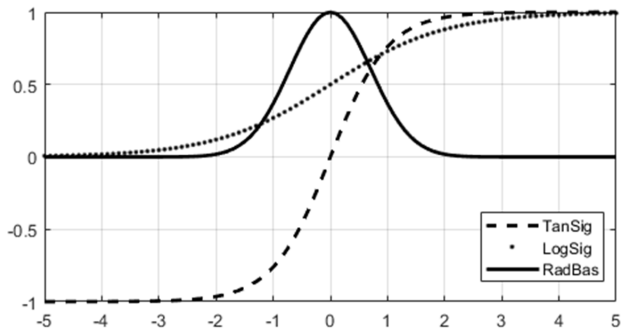

3.4.2. Mathematical representation

Let the inputs for MLP (with single hidden layer, 1..i hidden neurons and one output y), be x_k, where $k = 1, \ldots, K$ are multiplied by weights w_{ki} and summed up with the constant bias b_i. The resulting n_i in Equation (8) is the input to the activation function g

$$n_i = \sum_{j=1}^{K} w_{ji} x_j + b_i \tag{8}$$

Then the output of activation function g will be input into transfer function t; therefore, the output of network is calculated as in Equation (9):

$$\hat{y} = t(g(n_i)) = t\left(\sum_{j=1}^{m} w2_{ji} g\left(\sum_{k=1}^{K} w1_{kj} x_k + b1_j\right) + b2_j\right) \tag{9}$$

In our model, we have 60 inputs (20 bin histogram for each 3 regions) to predict one yield value in each year, introduced into MLP with one hidden layer of 5 hidden neurons, using 3 experiments of (activation-transfer) architecture, Equations (10)–(16).

Here, the output of node i becomes: $\forall x_j, j = 1, \ldots, 60 \;\; \exists g_i, i = 1, \ldots, 5$ *such that*

$$g_i = g\left(\sum_{j=1}^{60} w_{ji} x_j + bi\right) \tag{10}$$

1- Using TanSig as activation function and SatLin as transfer function:

$$tansig(n) = \frac{2}{(1 + e^{-2n})} - 1, \; purelin(n) = n$$

Therefore,

$$m = g_i = \frac{2}{1 + e^{-2\left(\sum_{j=1}^{60} w_{ji} x_j + b_i\right)}} - 1 \qquad -1 \le m \le 1,$$

$$i = 1, \ldots, 5 \tag{11}$$

And the output of MLP network $\hat{y}$ can be defined as:

$$\hat{y} = t(m) = \frac{2}{1 + e^{-2\left(\sum_{j=1}^{60} w_{ji} x_j + bi\right)}} - 1 \tag{12}$$

2- Using LogSig as activation function and PureLin as transfer function:

$$logsig(n) = \frac{1}{1 + e^{-n}}, \; purelin(n) = n$$

Therefore,

$$m = g_i = \frac{1}{1 + e^{-\left(\sum_{j=1}^{60} w_{ji} x_j + b_i\right)}} \qquad 0 \le m \le 1,$$

Table 1
The results of wheat and barley input data histogram

Crop		Wheat			Barley		
Hidden layer		Tansig	Logsig	Radbas	Tansig	Logsig	Radbas
Training (15 years)	MAE	0	0	0	0	0	0
	RMSE	0	0	0	0	0	0
	R^2	1.000	0.999	1.000	1.000	1.000	1.000
Test (4 years)	MAE	0.350	0.428	**0.230**	0.184	0.462	**0.126**
	RMSE	0.405	0.442	**0.236**	0.237	0.473	**0.158**
	R^2	0.764	0.890	**0.929**	0.864	0.993	**0.850**
Absolute err. of 2020		9.324	9.375	**1.059**	5.765	3.928	**1.895**

The eventual outcomes showed that the model that depends on the radial basis functions exceeds the rest models. Where the experiments on test samples showed a determination coefficient R^2 higher than 0.85 in both crops and an error level did not exceed 0.24.

$$i = 1, \ldots, 5 \tag{13}$$

And the output of MLP network $\hat{y}$ can be defined as:

$$\hat{y} = t(m) = \frac{1}{1 + e^{-\left(\sum_{j=1}^{60} w_{ji} x_j + b_i\right)}} \qquad 0 \le m \le 1,$$

$$i = 1, \ldots, 5 \tag{14}$$

3- Using RadBas as activation function and PureLin as transfer function:

$$radbas(n) = e^{-n^2},\ purelin(n) = n$$

Therefore,

$$m = g_i = e^{-\left(\sum_{j=1}^{60} w_{ji} x_j + b_i\right)^2} \qquad 0 \le m \le \infty,\ i = 1, \ldots, 5 \tag{15}$$

And the output of MLP network $\hat{y}$ can be defined as:

$$\hat{y} = t(m) = e^{-\left(\sum_{j=1}^{60} w_{ji} x_j + b_i\right)^2} \qquad 0 \le m \le 1,\ i = 1, \ldots, 5 \tag{16}$$

4. Performance Analysis and Results

The input/output data are divided into two main datasets, training data (containing data from the first 15 years) to train the ANN models and test data (containing data from the next 4 years) employed to evaluate the performance of the trained models on data not seen before by model. The tuned networks also are tested on the data of the 2020 year to test the trained neural networks by additional unseen data in order to evaluate the capability of the models under new conditions using absolute error (AE) as a metric.

Three statistical validation parameters were used for the comparisons of the predicted and observed results. The parameters were the root mean square error (RMSE), to measure the differences between predicted and actually observed values without indicating the direction of the deviation, in conjunction with mean absolute error (MAE), which is a linear score such that all the individual differences are weighted equally, and coefficient of determination (R^2) which measures the strength of the linear relationship between the predicted and actually observed values.

The evaluation results are reported in Table 1 for both crops wheat/barley. It showed that the coefficient of determination in all experiments reflects high results, in contrast to other measures MAE/RMSE that showed diverse results. The eventual outcomes showed that the model that depends on the radial basis functions exceeds the rest models. Where the experiments on test samples showed a determination coefficient R^2 is equal or higher than 0.85 in both crops and an error level did not exceed 0.24. Also, the additional unseen data of 2020 year proved the efficiency of radial basis neuron in learning features from normalized histogram of NDVI images. The AE of 2020 data was approximately 1 for wheat and 2 for barley.

5. Conclusion

This study revealed that it is possible to build a successful yield prediction model using a simple MLP technique and making it able to derive useful features and relationships capable of intelligent prediction by transforming the input into a more convenient form like a histogram that reflects more useful information. The proposed methodology greatly improved the performance compared to traditional approaches. This is attributed to some substantial remarkable characteristics of the model such as the segmentation of the study area into multi subregions based on the agricultural acquaintance of the region, and the model's ability the learning and understand the data based on transforming it into a more intelligent form able to reflect more useful information.

By analyzing the results of the experiments, the inference conclusion was that the barley in one way or another was more responsive to the model. Also, the radial basis functions outperform hyperbolic tangent sigmoid and logarithmic-sigmoid functions for the proposed ANN architectures.

Finally, the intention was to develop a powerful and flexible system for agriculture yield prediction based on analyzing remote sensing images in a more efficient methodology. The future development of work involves extending and applying the suggested methodology to a large-scale area that contains multiple crop yields under different agricultural conditions and testing the behavior of the model in this area.

Ethical Statement

This study does not contain any studies with human or animal subjects performed by any of the authors.

Conflicts of Interest

The authors declare that they have no conflicts of interest to this work.

Data Availability Statement

Data available on request from the corresponding author upon reasonable request.

References

[1] Lucani, P., & Saade, M. (2012). *Iraq: Agriculture sector note*. Italy: Food and Agriculture Organization.

[2] Burke, M., & Lobell, D. B. (2017). Satellite-based assessment of yield variation and its determinants in smallholder African systems. *Proceedings of the National Academy of Sciences, 114*(9), 2189–2194. https://doi.org/10.1073/pnas.1616919114

[3] Huete, A., Didan, K., Miura, T., Rodriguez, E. P., Gao, X., & Ferreira, L. G. (2002). Overview of the radiometric and biophysical performance of the MODIS vegetation indices. *Remote Sensing of Environment*, *83*(1–2), 195–213. https://doi.org/10.1016/S0034-4257(02)00096-2

[4] Heute, A. F., & Liu, H. Q. (1994). An error and sensitivity analysis of the atmospheric-and solid-collecting variants of the normalized difference vegetation index for the MODISEOS. *IEEE Transactions on Geoscience and Remote Sensing*, *32*, 897–905. https://doi.org/10.1109/36.298018

[5] Conradt, S., Bokusheva, R., Finger, R., & Kussaiynov, T. (2014). Yield trend estimation in the presence of farm heterogeneity and non-linear technological change. *Quarterly Journal of International Agriculture*, *53*(2), 121–140. https://doi.org/10.22004/ag.econ.195732

[6] MMPW (2014). *Structural plan for Diwaniyah stage 5 report*. Final report. Ministry of Municipalities and Public Works, Iraq.

[7] Didan, K. (2015). *MOD13Q1 MODIS/Terra vegetation indices 16-day L3 global 250m SIN grid v006* [Data set]. NASA EOSDIS land processes distributed active archive center. https://doi.org/10.5067/MODIS/MOD13Q1.006

[8] Xiao, X., Boles, S., Liu, J., Zhuang, D., Frolking, S., Li, C., & Moore III, B. (2005). Mapping paddy rice agriculture in southern China using multi-temporal MODIS images. *Remote Sensing of Environment*, *95*(4), 480–492. https://doi.org/10.1016/J.RSE.2004.12.009

[9] Lunetta, R. S., Knight, J. F., Ediriwickrema, J., Lyon, J. G., & Worthy, L. D. (2006). Land-cover change detection using multi-temporal MODIS NDVI data. *Remote Sensing of Environment*, *105*(2), 142–154. https://doi.org/10.1016/j.rse.2006.06.018

[10] Wardlow, B. D., Egbert, S. L., & Kastens, J. H. (2007). Analysis of time-series MODIS 250 m vegetation index data for crop classification in the US Central Great Plains. *Remote Sensing of Environment*, *108*(3), 290–310. https://doi.org/10.1016/j.rse.2006.11.021

[11] Friedl, M., & Sulla-Menashe, D. (2019). *MCD12Q1 MODIS/Terra+Aqua land cover type yearly L3 global 500m SIN grid v006* [Data set]. NASA EOSDIS land processes distributed active archive center. https://doi.org/10.5067/MODIS/MCD12Q1.006

[12] Liang, D., Zuo, Y., Huang, L., Zhao, J., Teng, L., & Yang, F. (2015). Evaluation of the consistency of MODIS Land Cover Product (MCD12Q1) based on Chinese 30 m GlobeLand30 datasets: A case study in Anhui Province, China. *ISPRS International Journal of Geo-Information*, *4*(4), 2519–2541. https://www.mdpi.com/2220-9964/4/4/2519

[13] Merritt, S. H., & Christensen, A. P. (2023). An experimental study of dimension reduction methods on machine learning algorithms with applications to psychometrics. *Advances in Artificial Intelligence and Machine Learning*, *3*(1), 760–777.

[14] Sun, J., Di, L., Sun, Z., Shen, Y., & Lai, Z. (2019). County-level soybean yield prediction using deep CNN-LSTM model. *Sensors*, *19*(20), 4363. https://doi.org/10.3390/s19204363

[15] Burger, W., & Burge, M. J. (2022). Histograms and image statistics. In W. Burger & M. J. Burger (Eds.), *Digital image processing: An algorithmic introduction* (pp. 29–48). Switzerland: Springer. https://doi.org/10.1007/978-1-4471-6684-9_3

[16] Haykin, S. (2009). *Neural networks and learning machines*. India: Pearson Education.

[17] Emam, A., Tonekabonipour, H., & Teshnelab, M. (2011). Applying MLP as a predictor and ANFIS as a classifier in ischemia detection via ECG. In *2011 IEEE International Conference on Systems, Man, and Cybernetics*, 2958–2962. https://doi.org/10.1109/ICSMC.2011.6084121

[18] Bishop, C. M. (1995). *Neural networks for pattern recognition*. USA: Oxford University Press.

[19] Mas, J. F., & Flores, J. J. (2008). The application of artificial neural networks to the analysis of remotely sensed data. *International Journal of Remote Sensing*, *29*(3), 617–663. https://doi.org/10.1080/01431160701352154

[20] Karul, C., Soyupak, S., Çilesiz, A. F., Akbay, N., & Germen, E. (2000). Case studies on the use of neural networks in eutrophication modeling. *Ecological Modelling*, *134*(2–3), 145–152. https://doi.org/10.1016/S0304-3800(00)00360-4

[21] Koivo, H. N. (2008). *Neural networks: Basics using matlab neural network toolbox*.

[22] Sharma, B., & Venugopalan, K. (2014). Comparison of neural network training functions for hematoma classification in brain CT images. *IOSR Journal of Computer Engineering*, *16*(1), 31–35.

How to Cite: Khalil, Z. H. & Hussein Khaleel, A. (2023). Design of a Multilayer Perceptron Network Based on the Normalized Histogram to Develop Yields Predictive Model. *Journal of Data Science and Intelligent Systems*. https://doi.org/10.47852/bonviewJDSIS32021359